Communications Earth & Environment https://doi.org/10.1038/s43247-026-03472-5

Article in Press

Phosphorus cycling dynamics in stratified low-phosphorus lakes

Received: 30 September 2025

Accepted: 20 March 2026

Cite this article as: Wei, Z., Wang, B., Yan, H. *et al.* Phosphorus cycling dynamics in stratified low-phosphorus lakes. *Commun Earth Environ* (2026). https://doi.org/10.1038/s43247-026-03472-5

Zhao Wei, Baoying Wang, Hao Yan, Longchen Zhu, Yu Wei, Yankai Shang & Huiming Bao

Phosphorus cycling dynamics in stratified low-phosphorus lakes

Zhao Wei[1,2], Baoying Wang[3], Hao Yan[1,2], Longchen Zhu[1,2], Yu Wei[1,2], Yankai Shang[1,2], Huiming Bao[1,2*]

1, International Center for Isotope Effects Research, State Key Laboratory of Critical Earth Material Cycling and Mineral Deposits, Nanjing University, Nanjing 210023, China

2, School of Earth Sciences and Engineering, Nanjing University, Nanjing 210023, China

3, State Key Laboratory of Pollution Control and Resource Reuse, School of the Environment, Nanjing University, Nanjing 210023, China

⁎ Corresponding author: Huiming Bao (bao@nju.edu.cn)

Abstract

Sustained eutrophication in low-phosphorus (P < 1 μM and phosphate (PO_4^{3-}) < 0.2 μM) lakes poses a challenge to understanding P cycling in stratified lakes. Conventional P concentration and low vertical-resolution phosphate oxygen isotope data ($\delta^{18}O_P$) cannot solve this problem. Here, we measured high-resolution $\delta^{18}O_P$ profiles in two typically low-P, eutrophic, thermally stratified lakes (Lake Hongfeng and Lake Aha, China) via a newly developed ESI-Orbitrap-MS technique. The lakes showed high $\delta^{18}O_P$ values (19.3‰-19.8‰) at the surface (0–2 m), but low values (13.4‰-13.7‰) at thermocline. A one-dimensional concentration-$\delta^{18}O_P$ coupled diffusion model constrains an apparent kinetic isotope effect of 0.9932 and 0.9906 for biological surface uptake and thermocline remineralization, respectively. The results suggest that eutrophication was sustained by a rapid PO_4^{3-} uptake by algae at surface and remineralization of organic P at depth. This study provides isotope evidence for P cycling dynamics in low-P natural lakes with excessive algae growth.

Introduction

Phosphorus (P) pollution drives eutrophication, which leads to harmful algal blooms, depletion of dissolved oxygen (DO), and mass mortality of fish and other aquatic life, ultimately destabilizing the entire aquatic ecosystem[1, 2, 3, 4]. Consequently, much effort has focused on reducing external (exogenous) P loads from sources such as agricultural runoff, industrial discharges, and urban sewage[5, 6]. Despite these measures, many lakes continue to experience eutrophication, with persistent blooms occurring even when ambient phosphate (PO_4^{3-}) concentrations are below the typical P limit ($P < 1$ μM and $PO_4^{3-} < 0.2$ μM)[7, 8, 9]. This persistence of eutrophication in seemingly P-limited lakes challenges the conventional notion that low PO_4^{3-} levels ensure ecosystem stability. However, there is currently a debate on the causes of eutrophication in low-P lakes. One prevailing hypothesis points to the internal loading of PO_4^{3-} from bottom sediments as a trigger for these blooms[10]. In thermally stratified lakes, however, this mechanism may not sustain eutrophication, as the thermocline may act as a strong physical barrier to the upward diffusion of sediment-released PO_4^{3-}. However, weeks-long, persistent eutrophication has been observed in some stratified low-P lakes in summer[11, 12]. Perhaps, advected subsurface nutrient tongue by discharge could import PO_4-rich intermediate waters laterally at a certain depth. Another likely P supply to the surface mixed layer is biological remineralization of sinking organic P, often concentrated near the base of the euphotic zone / upper thermocline[13,14]. Both the lateral discharge and the remineralization would result in a rise of PO_4^{3-} concentration at a certain depth and thus cannot be easily distinguished by PO_4^{3-} concentration profiles alone.

Phosphate oxygen isotope composition ($\delta^{18}O_P$) is a useful tool for studying the P cycle in ecosystems. Previous studies suggest that abiotic oxygen isotope exchange between PO_4^{3-} and water is negligible under ambient environment[15, 16, 17]. During biotic uptake of PO_4^{3-} in a starvation condition, microorganisms mainly rely on high-affinity transporters to uptake PO_4^{3-} from the ambient water, where light isotopologues are preferentially taken up,

leading to the enrichment (~3.3‰) of ^{18}O in the remaining PO_4^{3-} in solution[18, 19]. During organic P remineralization, kinetic oxygen isotope effects associated with the cleavage of the P-O bond and the incorporation of water-derived O in the formation of PO_4^{3-} result in lower than the equilibrium $\delta^{18}O_P$ value. The apparent kinetic isotope effect (*AKIE*) for PO_4^{3-} oxygen during the remineralization of phosphomonoester and phosphodiester, the main form of organic P in lake water, can result in ^{18}O-depleted PO_4^{3-}, with the degree of isotopic fractionation (i.e., 1000 (*AKIE*-1)) reaching -30‰ and -5‰, respectively[20, 21].

In a lake ecosystem, the $\delta^{18}O$ of PO_4^{3-} released from the sediment is typically higher or close to the equilibrium value, due to oxygen isotope exchange with porewater oxygen and limited exchange with the overlying lake-water that may have a different $\delta^{18}O_P$ or $\delta^{18}O$ of water value [13, 22, 23]. The utilization rate of PO_4^{3-} by microbial heterotrophs at depth is relatively lower than microbials in surface layer, and therefore its $\delta^{18}O_P$ value may remain constant at and below the thermocline. The two PO_4^{3-} source models, released from sediment at the bottom and remineralization of organic P near the thermocline, therefore, would predict distinguishable vertical $\delta^{18}O_P$ profiles that can be tested.

High-resolution vertical $\delta^{18}O_P$ data profile is required to conduct the test. However, the conventional method of thermal conversion/elemental analysis linked to a gas-source isotope ratio mass spectrometer (TC/EA–IRMS) requires collecting 25–50 L of water to generate sufficient silver phosphate (Ag_3PO_4) for $\delta^{18}O_P$ analysis[24, 25, 26]. Because of the analytical limitation, previous studies have only reduced the vertical resolution to > 5 m[14, 27], which would not be able to resolve a $\delta^{18}O_P$ profile in a stratified lake with a sharp thermocline. Here we employ an electrospray ionization Orbitrap mass spectrometry (ESI-Orbitrap-MS) technique recently developed by us for $\delta^{18}O_P$ analysis[28, 29]. The Orbitrap method reduces the sample amount by two to three orders of magnitude compared to the conventional method, i.e., 0.5-1 L vs 25-100 L. The obtained vertical PO_4^{3-} concentration and $\delta^{18}O_P$ data are then processed by a one-dimensional reaction-transport model to disentangle the uptake and release processes of lake PO_4^{3-} and to quantify

their respective *AKIE*.

Results

Lake water's physical and chemical parameters

Fig.1 illustrates the physical and chemical parameters of the water columns, including DO, pH, T, Chlorophyll-a (Chla), and Dissolved Organic Carbon (DOC). In the thermocline region, a sharp decline in DO is observed alongside an increase in DOC. In Lake Hongfeng, water T remains stable from 0 to 6 m in Lake Hongfeng (26.4 - 26.7 °C) and 0 to 4 m in Lake Aha (26.8 – 27 °C), respectively, drops sharply at 6 - 9 m and 6- 8 m, and further decreases to 23.5 °C to 24.8°C at 8 m to 9 m. The bottom T of the two lakes are 22.5 °C in Lake Hongfeng and 11.5 °C in Lake Aha, both accompanied by a drastic reduction in DO. Specifically, DO in Lake Hongfeng is 7.7 mg/L at the surface, then declines abruptly to 1.0 mg/L below the thermocline (at 9 m) and further to 0.3 mg/L at the water bottom. Similarly, in Lake Aha, DO is 9.3 mg/L at the surface, then drops sharply to 1.8 mg/L at 8 m, and reaches only 0.5 mg/L at the bottom. The surface pH is 8.2 in Lake Hongfeng and 7.8 in Lake Aha, decreasing to 7.3 at 9 m in Lake Hongfeng and 7.2 at 8 m in Lake Aha. The pH of Lake Hongfeng and continues to decrease gradually to 7.2 and 7.6 at the bottom. In Lake Hongfeng, the Chla concentration at the surface layer (0 - 2 m) reaches a maximum of 36.2 ppm before declining sharply to 1.4 ppm at the bottom. Similarly, in Lake Aha, the Chla concentration peaks at 39.4 ppm at the surface layer (0 - 2 m), and then decreases rapidly to 1.4 ppm at the bottom. Additionally, DOC in both lakes exhibits a pronounced increase within the thermocline. In Lake Hongfeng, DOC attains a maximum of 22.1 mg/L at a depth of 9 m, which is much higher than the concentrations observed in the upper and lower layers. In Lake Aha, the DOC peaks at 24.2 mg/L at the thermocline (8 m).

PO_4^{3-} Concentration and $\delta^{18}O_P$ profiles

PO_4^{3-} concentration in the two lakes exhibits a similar vertical pattern: low levels at the surface, an apparent increase in the middle, and an increase at the bottom (Table S1, Fig.2). Dissolved P (DP) concentration at 0 - 2 m was 0.1 to 0.2 μM at Lake Hongfeng and at ~0.1 μM in Lake Aha. At the thermocline, DP concentration increased to 0.5 μM in both lakes. In deeper water, DP concentration in Lake Aha rose from 0.3 μM at 18 m to 2.4 μM at 20 m, while in Lake Hongfeng, it remained at a low concentration between 0.2 and 0.4 μM at 18 to 19 m. Furthermore, the vertical concentration patterns of particulate P (PP), dissolved organic P (DOP), and total P (TP) in both lakes are positively correlated with those of DP (Fig.S1). Bottom TP concentration in Lake Aha (3.6 μM) was approximately four times higher than in Lake Hongfeng (1.0 μM).

$\delta^{18}O_P$ values in Lake Hongfeng and Lake Aha range from 13.4‰ to 19.7‰ and from 13.6‰ to 19.3‰, respectively (Fig.3 and Table S1). The highest $\delta^{18}O_P$ value was observed in Lake Hongfeng at 0 m (19.8‰) and in Lake Aha at 0.5 m (18.7‰), both of which deviate significantly from their calculated equilibrium values ($p < 0.01$), i.e., 14.3‰ for Lake Hongfeng and 14.4‰ for Lake Aha, considering the T and the $\delta^{18}O$ of lake water. At the thermocline—9 m in Lake Hongfeng and 8 m in Lake Aha—the $\delta^{18}O_P$ was at 13.4‰ and 13.6‰, respectively, which are lower than their corresponding equilibrium values (i.e., 14.5‰ for Lake Hongfeng and 14.7‰ for Lake Aha). In the bottom layer, the measured $\delta^{18}O_P$ in Lake Hongfeng and Lake Aha (16.9‰ and 15.5‰, respectively) once again deviates from their equilibrium values (i.e., 14.9‰ for Lake Hongfeng and 17.7‰ for Lake Aha).

Model constraint on PO_4^{3-} uptake and release processes

A one-dimensional transport-reaction model can provide quantitative constraints on PO_4^{3-} cycling processes in Lake Hongfeng and Lake Aha. The model considers sediment release, biological uptake, and organic P remineralization in shaping the observed P concentration and $\delta^{18}O_P$ profiles (detailed model formulation and

parameterization are described in the Methods section). The model-fitted maximum algal growth rate (μ_{max}) and the organic P mineralization rate (k_{org}) values are 0.18-0.44 1/h and 0.11-0.16 1/h in two lakes, respectively (Table 1). The concentration-fitted model was then used to fit the observed $\delta^{18}O_P$ profiles, by which the *AKIE* during PO_4^{3-} uptake ($AKIE_{uptake}$) were determined to be 0.9932 in Lake Hongfeng and 0.9929 in Lake Aha (Table 1, Fig. 2b and 2d), and the *AKIE* during organic P remineralization ($AKIE_{org}$) were 0.9906 in Lake Hongfeng and 0.9900 in Lake Aha.

Collectively, the physicochemical data and the high-resolution $\delta^{18}O_P$ profiles presented in the Results section provide a foundation for distinguishing the source of PO_4^{3-} driving eutrophication in these low-P systems.

Discussion

Oxygen isotope effect during phosphate uptake

The $\delta^{18}O_P$ values at the surface of the two lakes are apparently higher than the equilibrium values (e.g., 19.7‰ vs. the equilibrium value of 14.2‰ at 0 m in Lake Hongfeng). Notably, the model-constrained *AKIE*, alternatively expressed as 1000($AKIE_{uptake}$-1), -7.1‰ to -6.8‰ at the surface of the two lakes, are much bigger than those reported from laboratory culture experiments (~ -3.3‰) [18, 19]. Sensitivity analysis shows that when $AKIE_{uptake}$ ranges from 0.989 to 0.997, the surface $\delta^{18}O_P$ of Lake Hongfeng and Lake Aha changes the most, with variation ranges of 14.2‰-22.9‰ and 14.3‰-23.7‰, respectively (Fig. S2a and S2b). Studies have shown that when PO_4^{3-} concentration is <200 μM, algal cells activate an efficient uptake mechanism mediated by the high-affinity PO_4^{3-} transporters, e.g., PstC and PstA[18]. When PO_4^{3-} concentration is < 1 μM, the genes of the relevant P uptake and high-affinity PO_4^{3-} transport systems (phoX, sphX, and pstSCAB) show an up-regulation in transcription abundance by 1.8 - 49 fold[30, 31]. *AKIE* may occur due to cell activity under P limitation when the high-affinity PO_4^{3-} transporters are upregulated. However, in this study, the PO_4^{3-} concentration in the surface waters of the two lakes is at ~0.1 μM, 3–4 orders of magnitude lower than in the laboratory culture experiments (200 to 1000 μM)[18, 19]. During the biotic uptake of PO_4^{3-}, P-O bond

is broken [32, 33], and thus the light isotope ^{16}O is preferentially incorporated into biological organic P (such as ATP and nucleic acids), resulting in the enrichment of ^{18}O in the remaining aqueous-phase PO_4^{3-} [18, 19]. The *AKIE* would be amplified by the small reservoir of PO_4^{3-} in the extremely low-P surface water.

Given the low TP concentration (P < 0.5 μM) in the surface, we ruled out the possibility of external P input. Notably, this is not the first time the *AKIE* of $\delta^{18}O_P$ has been observed in the field. Li, Bai [27] observed that surface water $\delta^{18}O_P$ in September (21.3‰) was ~5‰ higher than the equilibrium value (16.1‰) during their seasonal monitoring of vertical profiles in Chesapeake Bay. However, the bay's intense hydrodynamic mixing (relative to reservoirs) and lower resolution sampling (30 m vertical intervals) prevented the determination of the uptake *AKIE*. Similar processes occur in other ecosystems, e.g., soil-plant systems[34, 35]. However, rapid rates of metabolism in these systems accelerate ^{18}O exchange, complicating the determination of *AKIE* dynamics during PO_4^{3-} uptake. Our study revealed that a larger AKIE can be manifested in a low-P environment, likely due to a combination of specialized PO_4^{3-} transporters and a reservoir effect. In other P-starved environments (such as the polar tundra or the deep ocean), plants or microorganisms typically maximize their P acquisition capacity by actively regulating relevant gene expression or altering root architecture [36, 37]. The correlation between this highly efficient P utilization strategy and isotope fractionation suggests that AKIE could potentially serve as an indicator of the degree of P limitation in ecosystems, offering a new perspective for understanding the dynamics of P cycling.

Phosphate oxygen kinetic isotope effect during remineralization of organic P

Chla concentration in both lakes (10 mg/L < Chla < 50 mg/L) indicates that the lakes are in a state of moderate eutrophication. The low $\delta^{18}O_P$ and high PO_4^{3-} concentration in the thermocline of the two lakes support an intense remineralization of organic P, which was the source of the added PO_4^{3-}. The $\delta^{18}O_P$ values in the thermocline (13.4‰ in Lake Hongfeng and 13.6‰ in Lake Aha) are lower than the predicted equilibrium values (14.6‰ in Lake Hongfeng

and 14.7‰ in Lake Aha). Model results show that the remineralization *AKIE*, -10.0‰ to -9.4‰ in the form of 1000($AKIE_{org}$-1), of the two lakes are within the range of -30.0‰ to -5.0‰ as reported by previous laboratory experiments. Meanwhile, the remineralization rates (k_{org}) of the two lakes (0.11-0.16 μM/h) were higher than those of the oligotrophic lakes (0.009-0.075 μM/h)[38]. Sensitivity analysis reveals that when $AKIE_{org}$ ranges from 0.982 to 0.990, the $\delta^{18}O_P$ at the thermocline of Lake Hongfeng and Lake Aha varies from 8.1‰ to 14.5‰ and from 7.0‰ to 14.2‰, respectively (Fig. S2c and S2d). Our interpretation is that in thermally stratified region, the upper layer exhibits lower density than the lower layer, leading to the accumulation of sinking particles (e.g., dead algal cells). In this region, there is also an increase in the concentration of DOC (36.6 mg/L at 10 m in Lake Hongfeng and 22.1 mg/L at 8 m in Lake Aha), reflecting a large substrate pool that fuels intense microbial remineralization[39, 40]. These enzymes preferentially cleave P from organic matter over carbon. The rate of PO_4^{3-} release through microbial remineralization of sinking biomass has exceeded the rate of PO_4^{3-} uptake. Consequently, this efficient recycling mechanism ensures that the rate of PO_4^{3-}release from sinking biomass consistently outpaces its microbial uptake[41]. Although PO_4^{3-} derived from organic P remineralization has been repeatedly invoked in eutrophic water bodies, it has long been difficult to distinguish them from PO_4^{3-} derived from sediments due to low-vertical sampling resolution [13, 27, 42]. Here, our Orbitrap-MS measured high-vertical-resolution $\delta^{18}O_P$ profiles support the model that PO_4^{3-} derived from organic P remineralization near the thermocline sustained the eutrophication observed in the surface water body in the summer.

Phosphate released from the sediment-water interface

The $\delta^{18}O_P$ values below the thermocline in Lake Hongfeng are higher, while in Lake Aha are lower than the predicted equilibrium values (Fig. 2b and Fig. 2d). This difference may be caused by the different $\delta^{18}O_P$ values of PO_4^{3-} released from sediments. The $\delta^{18}O_P$ values of the bottom sediments, 17.1‰±0.3‰ at Lake Hongfeng and 15.8‰±0.2‰ at Lake Aha (Table S1), are close to the measured values below the thermocline, supporting that the

release of inorganic P from the sediment was the main source of PO_4^{3-} supplied to the deep water. Apparently, these sediment stored PO_4^{3-} have not reached oxygen isotope equilibrium with their ambient water and the thermal stratification helped maintain the relatively high concentration of PO_4^{3-} in deep water and prevented it from diffusing above the thermocline. However, this high PO_4^{3-} concentration in the lake bottom can be the initial trigger of eutrophication or a continuous PO_4^{3-} source within the lake over a long time scale.

Isotopic insights into the dynamics of P cycling

In contrast to previous studies that relied solely on concentration gradients, our $\delta^{18}O_P$ profile provides isotopic insights into the P uptake by algae and remineralization of organic P pathways. By integrating the vertical distribution of $\delta^{18}O_P$ with a one-dimensional vertical diffusion model, we reveal a P cycling mechanism dominated by a rapid and efficient algae P uptake and remineralization of organic P (Fig. 3). The cycle begins in the sunlit surface water, where a rapid algal growth drives an intense uptake of PO_4^{3-}. This biological uptake imparts a large apparent *AKIE*, resulting in highly enriched $\delta^{18}O_P$ (18.0‰–19.8‰) in the remaining P pool (Fig. 4). Upon death, this newly formed algal biomass, now in the form of organic P, sinks from the surface layer. The thermocline acts as a critical biogeochemical barrier and reactor, where sinking organic matter is intercepted and accumulates and undergoes a rapid remineralization that is associated with a large isotope fractionation as well (1000(*AKIE*org-1): -10.0‰ to -9.4‰), resulting in lower $\delta^{18}O_P$ values (13.4‰–13.7‰) (Fig. 4). This process efficiently converts particulate organic P back into bioavailable PO_4^{3-}. The regenerated PO_4^{3-} is then readily reintroduced into the surface layer, establishing a self-sustaining feedback loop where the products of the algal bloom become the primary fuel for its continuation. In contrast, the P released from the sediment-water interface ($\delta^{18}O_P$ 15.7‰–17.1‰) is largely isolated from the surface water by thermal stratification (Fig. 3). This physical barrier effectively decouples the surface from the larger

sedimentary P reservoir. Consequently, the rapid internal recycling at the thermocline becomes the dominant P supply pathway, sustaining the algal blooms in the upper water.

The $\delta^{18}O_P$ profile allows for isolating and quantitatively assessing the relative rates of key P cycling processes, including organic P remineralization and sediment release. This capability provides a data-driven foundation required to design and implement highly targeted remediation strategies (e.g., hypolimnetic aeration or sediment capping). Ultimately, by providing a mechanistic understanding of spatially resolved P recycling, this approach enhances the reliability of predictive models used to forecast future trophic status and effectively prevent eutrophic conditions. As global warming intensifies thermal stratification, the rapid water-column P recycling identified here may become a dominant driver of eutrophication in thousands of low-P lakes globally.

Conclusions

Surface water eutrophication in stratified lakes requires a steady supply of PO_4^{3-}. In lakes with a low PO_4^{3-} concentration, the PO_4^{3-} supply can come from upward diffusion through the thermocline, release from sediment, or from a rapid remineralization of organic P in the surface mixed layer. This study used high-resolution vertical lake-water $\delta^{18}O_P$ profiles measured by an ESI-Orbitrap-MS method. Combining with PO_4^{3-} concentration and other chemical and physical parameters, we obtained 1000(*AKIE*-1) values for PO_4^{3-} oxygen at ~ -7‰ and ~ -10‰, respectively, during biotic uptake at the surface and during remineralization of organic P near the thermocline. The result supports that rapid remineralization of organic P in the stratified zone supplies PO_4^{3-} to the upper layers, promoting the rapid growth of algae during summer stratification. Sediment releases PO_4^{3-} with distinct $\delta^{18}O_P$ values and may be the trigger but not the sustained P source for the eutrophication.

Methods

Study Area

Water column samples were collected from Lake Aha (26°32′ N, 106°39′ E) and Lake Hongfeng (26°26'N, 106°19'E) in Guiyang City, Guizhou Province, Southwestern China. All samples were collected in July during a stratification period when eutrophication occurred. The sampling locations are shown in Fig.5a. The depths of Lake Aha and Lake Hongfeng are 20 m and 19 m, respectively. Both lakes are located on the Yunnan-Guizhou Plateau and have a subtropical humid monsoon climate. Both lakes are well-known low-P eutrophic lakes. To avoid interference between the upper and lower layers during the vertical sampling process, a stopper-type deep-water sampler (HYDRO-BIOS, Germany) was used to collect about 1.5 L of water samples at 2 m intervals in Lake Aha and at 1 m intervals in Lake Hongfeng. Additionally, about 1.5 L of water samples were collected from the surface (0 m) and 0.5 m below the surface in each lake. In situ measurements of water column parameters, including T, DO, and pH, were conducted using a multi-parameter water quality meter (EXO, YSI, USA). We collected 33 water samples and 2 sediment samples. Upon returning to the laboratory, all samples were immediately filtered and stored in a refrigerator at -4°C for future use.

Determination of Chla and DOC

The concentration of Chla in water samples was determined using the hot ethanol extraction method[43]. In this procedure, 90% ethanol was preheated in a water bath maintained at 80–85 °C. A filter membrane containing Chla was placed in a 10 mL centrifuge tube, and 6–8 mL of the heated ethanol was added to ensure complete submersion of the membrane. The tube was incubated in the water bath for 2 min and then left for approximately 5 h for extraction in the dark. After extraction, the filter membrane was carefully wrung out with forceps, and the extract was subsequently filtered through a 0.45 μm syringe filter into a 10-mL graduated test tube for accurate volume measurement. Next, using 90% ethanol as a reference, the extract was analyzed at wavelengths of 665 nm and 750 nm

with a spectrophotometer (UV2550, Shimadzu, Japan). Following the initial colorimetric measurement, approximately 50 μL of 1 M hydrochloric acid was added to the cuvette, and the reaction was allowed to proceed for 1 minute before a second colorimetric analysis. The concentration of Chla in the water sample was then calculated using the following equation (1):

$$c(\text{Chla}) = \frac{27.9(E_a - E_b)V_e}{V} \quad (1)$$

Where, c(Chla) is the Chla concentration (mg/L). E_a and E_b denote the differences in optical density before and after acidification at 665 nm and 750 nm, respectively. Here, V_e indicates the extract volume (mL), and V represents the volume of the filtered water sample (L). After filtering the water samples through a 0.22 μm membrane, the DOC was measured using a total organic carbon analyzer (Elementar, Germany).

Determination of P Concentration

For TP content, a 5 mL water sample was transferred into a digestion tube and supplemented with 2 mL of a 5% potassium persulfate solution. The tube was then subjected to high-pressure steam sterilization and digested at 121°C for 30 min, converting all forms of organic P into PO_4^{3-}. The dissolved total P (DTP) was measured using the same procedure and applied instead to a filtered water sample. DP was defined as the PO_4^{3-} content in the filtrate obtained after passing the water sample through a 0.45-μm filter, as the same to PO_4^{3-} in water. DOP was inferred by subtracting the DP value from the DTP content. PP was determined by subtracting the DTP value from the TP content. All analyses were conducted using the ammonium molybdate spectrophotometric method, with absorbance measured at 700 nm, as described by Murphy and Riley [44]. Blank tests were performed on each batch of samples throughout the chemical analysis to ensure the accuracy and reliability of the results.

Isotope Pretreatment and Analysis

The $\delta^{18}O$ values of the water samples ($\delta^{18}O_w$) were determined using a laser-based LGR IWA-45EP instrument (LGR, Canada) following filtration through a 0.22 μm membrane. In the sediment, $\delta^{18}O_P$ was obtained according to Liu, Wang [45]. PO_4^{3-} in the sediment was extracted using 1M HCl, and PO_4^{3-} was enriched and impurities were removed using Zirconium oxide gel (ZrO-gel) to obtain pure Ag_3PO_4. We used a Thermal Conversion/Elemental Analyzer to convert Ag_3PO_4 at 1410°C to CO gas, then the $\delta^{18}O$ of the CO was measured by the TC/EA-IRMS (Thermo Fisher Scientific Delta V Plus, USA). The standard deviation (1 SD) of the $\delta^{18}O_P$ by TC/EA-IRMS measurements was 0.4‰. The freshwater sample pretreatment and $\delta^{18}O_P$ analysis were conducted by the protocol described as follows: Initially, 1 L of the filtered sample was collected, and 5-10 self-fabricated ZrO-gel membranes were added. The resulting mixture was agitated at a constant speed of 100 rpm for 48 h, during which the selective adsorption properties of the ZrO-gel membranes facilitated the pre-enrichment of PO_4^{3-}. After enrichment, the membranes were removed and immersed in 10 mL of 1 M NaOH solution, followed by shaking for an additional 24 h to elute PO_4^{3-} into the liquid phase, thereby preliminarily removing impurities. The resultant eluent was subsequently passed through an 8-mL AG50W-X8 cation exchange resin column (hydrogen form, 100–200 mesh, biotechnology grade, Bio-Rad, USA), where an exchange reaction between Na^+ and H^+ generated water while the residual H^+ combined with anions such as NO_3^-, SO_4^{2-}, and Cl^-. Thereafter, the AG1-X8 anion exchange resin (hydroxide form, 100–200 mesh, biotechnology grade, Bio-Rad, USA) was pre-treated by pumping 40 mL of 1 M $NaHCO_3$ solution through a 3 mL column at a flow rate of 1.5 mL/min using a peristaltic pump, followed by rinsing with 60 mL of 18.2 MΩ ultrapure water at the same rate. Once the pretreatment was complete, the processed sample was loaded into a 60 mL syringe and passed through the AG1-X8 resin column for further enrichment and purification of PO_4^{3-}. Subsequently, a 45 mL aliquot of 0.15 M $NaHCO_3$ solution was passed through the column at a flow rate of 1.5 mL/min to elute PO_4^{3-}, with fractions collected between 9 and 21 mL. The collected solution was dried using a vacuum centrifugal concentrator (miVac Duo, Genevac,

UK), and then 10 μL of 18.2 MΩ ultrapure water to redissolve the PO_4^{3-}. Then adding 0.99 mL of methanol to yield a 1 mL of PO_4^{3-} at a concentration of 50 μM for subsequent ESI–Orbitrap–MS (Eclipse, Thermo Fisher Scientific, USA) analysis. Additionally, to meet the requirements for isotope analysis, a 1 mL solution containing 50 μM PO_4^{3-} in a methanol–water matrix with 50 nmol PO_4^{3-} was prepared. The detailed procedure is illustrated in Fig. 5b, and the purified concentration and volume of PO_4^{3-} are provided in Table S2[29].

$\delta^{18}O_P$ of freshwater was measured using an ESI–Orbitrap–MS equipped with a dual-injection system. This methodology was optimized based on previous research findings[28]. During analysis, the dual-injection system was precisely maintained at a flow rate of 5 μL/min to ensure the stable introduction of both the standard reference and sample solutions into the mass spectrometer. The PO_4^{3-} solution concentration was rigorously controlled at 50 μM to preserve the accuracy and comparability of the results. To minimize interference from solution mixing, an alternating injection procedure was implemented: the standard reference and sample solutions were alternately injected every 10 min, with each switch preceded by a 3 min interval designated for system cleaning and stabilization, followed by a 7 min analytical period. The entire process spanned 70 min with additional ESI–Orbitrap–MS parameters listed in Table S3. The $\delta^{18}O_P$ scale was calibrated against community-shared standards, specifically using three international standards: B2207 (Ag_3PO_4, $\delta^{18}O_P$=21.7‰, Vienna Standard Mean Ocean Water (VSMOW)), USGS80 (Ag_3PO_4, $\delta^{18}O_P$=13.1‰, VSMOW), and USGS81 (Ag_3PO_4, $\delta^{18}O_P$=35.4‰, VSMOW). International standards (Ag_3PO_4) were converted to NaH_2PO_4 solutions through dissolution in ammonia, cation exchange (AG50W-X8 resin), and pH adjustment to 7.0[29]. The standard deviation (1 SD) of the $\delta^{18}O_P$ measured by ESI-Orbitrap-MS was 0.8‰, as was reported in our previous study[28, 29]. Data processing was conducted using IsoX software (Thermo Fisher Scientific, USA) to extract ion intensities from RAW files and convert them into ion counts. The oxygen isotope ratios were directly calculated from the IsoX output via the IsoXL website (version 0.53). The calibration curve of the international

standard sample is shown in Fig.S3.

In validating isotopic fractionation equilibrium for identifying P sources in watersheds using $\delta^{18}O_P$, the central premise is that the oxygen in river water PO_4^{3-} does not reach isotopic fractionation equilibrium with the oxygen in H_2O. The calculation relies on equation (2) provided by[46],

$$\delta^{18}O_{Eq} = (\delta^{18}O_W + 1000)e^{(14.43\times(1000/T) - 26.54)/1000} - 1000 \quad (2)$$

Where $\delta^{18}O_{Eq}$ denotes the oxygen isotope ratio of PO_4^{3-} under equilibrium conditions, T represents the temperature in Kelvin (K), and $\delta^{18}O_w$ corresponds to the oxygen isotope ratio in the overlying water. With known values of $\delta^{18}O_w$ and T, $\delta^{18}O_{Eq}$ can be calculated, and by comparing this computed value with the measured $\delta^{18}O_P$, it is possible to assess whether isotopic fractionation equilibrium has been achieved between the oxygen in PO_4^{3-} and the overlying water.

Diffusion - Reaction Model

To simulate the distribution of PO_4^{3-} and $\delta^{18}O_P$ in two lakes, a one-dimensional diffusion model based on the finite-difference method was established in this study. This model comprehensively considers the impacts of various physical and biogeochemical processes on the distribution of and their isotopes, including diffusion, PO_4^{3-} uptake by algae, organic P mineralization, and sediment PO_4^{3-} release.

Model based on vertical one-dimensional diffusion

The calculation formulas for the steady-state PO_4^{3-} concentration and $\delta^{18}O_P$ distribution are shown in equation (3-5):

$$\frac{\partial C}{\partial t} = D\frac{\partial^2 C}{\partial z^2} - U(z,t) + R_m(z,t) + R_s \quad (3)$$

$$\frac{\partial C_{18_O}}{\partial t} = D\frac{\partial^2 C_{18_O}}{\partial z^2} - U_{18_O}(z,t) + R_{m_{18_O}}(z,t) + R_{s_{18_O}} \quad (4)$$

$$\frac{\partial C_{16_O}}{\partial t} = D\frac{\partial^2 C_{16_O}}{\partial z^2} - U_{16_O}(z,t) + R_{m_{16_O}}(z,t) + R_{s_{16_O}} \quad (5)$$

Where D represents the diffusion coefficient with a value of 0.0036 m^2/h, this coefficient characterizes the diffusion ability of PO_4^{3-} and its isotopes in water, taking the diffusion of SO_4^{2-} in the water as a reference[47]. U, U_{18O}, and U_{16O} are the utilization fluxes of PO_4^{3-}, ^{18}O, and ^{16}O by algae, respectively. R_m, $R_{m_{18_O}}$, and $R_{m_{18_O}}$ are the release flux of PO_4^{3-}, ^{18}O, and ^{16}O from organic P mineralization, respectively. Rs, Rs_{18O}, and Rs_{16O} are the release rates of PO_4^{3-}, ^{18}O, and ^{16}O from sediment release, respectively. The uptake of PO_4^{3-} is considered in conjunction with both PO_4^{3-} and Chla simultaneously. It is modified according to the Monod formula for algal growth and expressed as equation (6):

$$U = \mu_{max} \times \frac{\mathrm{c(Chla)}}{K_{\mathrm{Chla}} + \mathrm{c(Chla)}} \times \frac{\mathrm{c}(PO_4^{3-})}{K_{PO_4^{3-}} + \mathrm{c}(PO_4^{3-})} \quad (6)$$

Where μ_{max} is the maximum specific growth rate of algae. K_{Chla} is the half-saturation constant for Chla, with a value of 0.05 in both lakes[48]. It represents the concentration of Chla when U is half of its maximum value. $K_{PO_4^{3-}}$ is the half-saturation constant for PO_4^{3-}, having a value of 0.1 μM in both lakes[48]. Considering isotopic fractionation, the current ratio of $^{18}O/^{16}O$ (R) value becomes $R' = R \times AKIE_{uptake}$ after the fractionation process, where c denotes the $\delta^{18}O_P$ fractionation factor for algal utilization.. Consequently, $U_{18O} = U \times R'/(1+R')$, and $U_{16O} = U - U_{18O}$. During the organic P mineralization process, the rate of PO_4^{3-} release is directly proportional to the concentration of DOP, described by equation (7).

$$R_{\mathrm{m}} = k_{\mathrm{org}} \times c(P_{\mathrm{org}}) \quad (7)$$

Here, k_{org} represents the organic P mineralization rate constant (1/h). Before the onset of the organic P mineralization process, the R_m value in the current water body is transformed to $R_m' = R_m \times AKIE_{org}$ after fractionation, where $AKIE_{org}$ is the fractionation factor for organic P mineralization. $R_{m18O} = R_m \times R_m'/(1+R_m')$, and $R_{m16O} = R_m - R_{m18O}$.

The sediment release process is set in the bottom area of the lake. The release rate increases linearly with depth, which can be expressed as equation (8):

$$R_s = k_s \times c(PO_4^{3-}{}_{bottom}) \quad (8)$$

Where k_s is the sediment release rate constant (1/h). In Lake Hongfeng, the k_s is 0.016 μM/h, and in Lake Aha it is 0.1μM/h[49, 50]. For isotope-related calculations: $R_{s_{18_O}}$=R_S×R_{bottom}/(1+R_{bottom}), and $R_{s_{16_O}}$=R_S-$R_{s_{18_O}}$. Among them, R_{bottom}=($\delta^{18}O_{bottom}$/1000+1)×$R_{standard}$, and $\delta^{18}O_{bottom}$ represents the isotope value of bottom diffusion (‰), $R_{standard}$ refers to the isotopic ratio of ^{18}O to ^{16}O in a standard substance..

Model calculation and simulation process

We employed the Differential Evolution global optimization algorithm (DEoptim package in R) to find the optimal parameter set. The key parameters in the model (including μ_{max}, k_{org}, $AKIE_{uptake,}$ and $AKIE_{org}$) were determined by this optimization algorithm. Within the model's numerical integration, the spatial gradients of PO_4^{3-} concentration and its $\delta^{18}O_P$ are calculated based on the net balance of these biogeochemical fluxes and the vertical mixing coefficient. The concentration values for the next node above are then updated according to these gradients, thereby constructing the complete vertical profiles. The final optimized parameters are summarized in Table 1.

Sensitivity analysis

To quantify the impact of $AKIE_{uptake}$ and $AKIE_{org}$ on the vertical profile of $\delta^{18}O_P$, the baseline values of $AKIE_{uptake}$ and $AKIE_{org}$ were extracted based on the optimal parameters obtained from DEoptim optimization. A simultaneous offset of ±0.002 was applied to $AKIE_{uptake}$ and $AKIE_{org}$, with only these parameters modified while keeping other parameters at their optimal values. Meanwhile, the simulated profiles of $\delta^{18}O_P$ under each offset were generated.

Statistical analysis

Statistical comparisons between measured $\delta^{18}O_P$ and $\delta^{18}O_{Eq}$ were conducted using paired-sample t-tests. Independent-sample t-tests were used to distinguish surface (depth ≤ 1 cm) and subsurface layers. All analyses were performed in R.

Acknowledgments

This study was supported by the National Natural Science Foundation of China (W2441015, 42494851, 42273032), Fundamental Research Funds for the Central Universities, including the General Program (0206/14380232, 0206/14380918), and additional grants (0206/14380204, 0206/14380150, 0206/14380185, and 0206/14380174), as well as startup fund from Nanjing University to HB.

Conflict of interest

The authors declare that they have no known competing financial interests or personal relationships that could have appeared to influence the work reported in this paper.

Data availability

All data generated for figures in this study have been deposited in figshare: https://doi.org/10.6084/m9.figshare.31566028.

Code Availability

All custom R code used in this study is freely available without restriction on Zenodo at https://doi.org/10.5281/zenodo.19031192.

Author contributions

Z.W. and H.B. conceived the research idea and design. Z.W. collected water samples and Lake-water chemistry data with the assistance from B.W. Z.W., Y. S. and H. Y.. Z.W and L.Z conducted the Orbitrap-MS-based $\delta^{18}O_P$ analyses. Z.W. H.Y and H.B analyzed the results. Z.W. and Y.W. assisted in the 1-D data modeling. Z.W. and H.B. wrote the paper with all co-authors contributed to the revisions.

Reference:

1. Duhamel S. The microbial phosphorus cycle in aquatic ecosystems. *Nat Rev Microbiol* 2025, **23**(4)**:** 239-255.

2. Feng L, Wang Y, Hou X, Qin B, Kuster T, Qu F*, et al.* Harmful algal blooms in inland waters. *Nat Rev Earth Environ* 2024, **5**(9)**:** 631-644.

3. Kosten S, Huszar VLM, Bécares E, Costa LS, van Donk E, Hansson LA*, et al.* Warmer climates boost cyanobacterial dominance in shallow lakes. *Global Change Biology* 2012, **18**(1)**:** 118-126.

4. Qin BQ, Deng JM, Shi K, Wang J, Brookes J, Zhou J*, et al.* Extreme Climate Anomalies Enhancing Cyanobacterial Blooms in Eutrophic Lake Taihu, China. *Water Resources Research* 2021, **57**(7)**:** e2020WR029371.

5. Zhong QM, Huang RX, Yu YD, Feng CY, Liang S. Phosphorus emissions from changing phosphorus supply chain networks in China. *Journal of Cleaner Production* 2022, **369:** 133259.

6. Basu NB, Singh N, Van Meter K. Dissolved phosphorus concentrations are increasing in streams across the Great Lakes Basin. *Nature Geoscience* 2023, **16**(10)**:** 841-842.

7. Cao X, Wang Y, He J, Luo X, Zheng Z. Phosphorus mobility among sediments, water and cyanobacteria enhanced by cyanobacteria blooms in eutrophic Lake Dianchi. *Environmental Pollution* 2016, **219:** 580-587.

8. Cao J, Wu Y, Li Z-k, Hou Z-y, Wu T-h, Chu Z-s*, et al.* Dependence of evolution of Cyanobacteria superiority on temperature and nutrient use efficiency in a meso-eutrophic plateau lake. *Science of The Total Environment* 2024, **927:** 172338.

9. Müller B, Steinsberger T, Schwefel R, Gächter R, Sturm M, Wüest A. Oxygen consumption in seasonally stratified lakes decreases only below a marginal phosphorus threshold. *Scientific Reports* 2019, **9**(1)**:** 18054.

10. Kirol AP, Morales-Williams AM, Braun DC, Marti CL, Pierson OE, Wagner KJ*, et al.* Linking Sediment and Water Column Phosphorus Dynamics to Oxygen, Temperature, and Aeration in Shallow Eutrophic Lakes. 2024, **60**(1)**:** e2023WR034813.

11. Kamarainen AM, Penczykowski RM, Van de Bogert MC, Hanson PC, Carpenter SR. Phosphorus sources and demand during summer in a eutrophic lake. *Aquatic Sciences* 2009, **71**(2)**:** 214-227.

12. Duan Z, Liang J, Shi L, Xu Y, Gao W, Tan X. Eutrophication Heterogeneously Enhances Organic Matter

and Phosphorus Exchanges among Dissolved, Particulate, and Sedimentary Phases in a Large Shallow Lake. *Environmental Science & Technology* 2025, **59**(26)**:** 13264-13274.

13. Joshi SR, Kukkadapu RK, Burdige DJ, Bowden ME, Sparks DL, Jaisi DP. Organic Matter Remineralization Predominates Phosphorus Cycling in the Mid-Bay Sediments in the Chesapeake Bay. *Environmental Science & Technology* 2015, **49**(10)**:** 5887-5896.

14. Elsbury KE, Paytan A, Ostrom NE, Kendall C, Young MB, McLaughlin K*, et al.* Using oxygen isotopes of phosphate to trace phosphorus sources and cycling in Lake Erie. *Environ Sci Technol* 2009, **43**(9)**:** 3108-3114.

15. Longinelli A, Bartelloni M, Cortecci G. The isotopic cycle of oceanic phosphate, I. *Earth and Planetary Science Letters* 1976, **32**(2)**:** 389-392.

16. Blake RE, O'Neil JR, Garcia GA. Oxygen isotope systematics of biologically mediated reactions of phosphate: I. Microbial degradation of organophosphorus compounds. *Geochimica et Cosmochimica Acta* 1997, **61**(20)**:** 4411-4422.

17. O'Neil JR, Vennemann TW, McKenzie WF. Effects of speciation on equilibrium fractionations and rates of oxygen isotope exchange between (PO4)aq and H2O. *Geochimica et Cosmochimica Acta* 2003, **67**(17)**:** 3135-3144.

18. Blake RE, O'Neil JR, Surkov AV. Biogeochemical cycling of phosphorus: Insights from oxygen isotope effects of phosphoenzymes. *American Journal of Science* 2005, **305**(6-8)**:** 596-620.

19. Lis H, Weiner T, Pitt FD, Keren N, Angert A. Phosphate Uptake by Cyanobacteria Is Associated with Kinetic Fractionation of Phosphate Oxygen Isotopes. *Acs Earth and Space Chemistry* 2019, **3**(2)**:** 233-239.

20. Colman AS, Blake RE, Karl DM, Fogel ML, Turekian KK. Marine phosphate oxygen isotopes and organic matter remineralization in the oceans. *Proc Natl Acad Sci U S A* 2005, **102**(37)**:** 13023-13028.

21. Liang Y, Blake RE. Oxygen isotope signature of P regeneration from organic compounds by phosphomonoesterases and photooxidation. *Geochimica Et Cosmochimica Acta* 2006, **70**(15)**:** 3957-3969.

22. Yuan H, Wang H, Cai Y, Yin H, Zeng Q, Liu E*, et al.* Iron bound phosphorus predominates the contribution of phosphorus to lake system from terrigenous source: The evidence from the small watershed scale. *Water Research* 2023, **245:** 120661.

23. Jin Z, Wang J, Zhang R, Liao P, Liu Y, Yang J*, et al.* Identification of the sources of different phosphorus

fractions in lake sediments by oxygen isotopic composition of phosphate. *Applied Geochemistry* 2023, **151:** 105627.

24. Ishida T, Uehara Y, Iwata T, Cid-Andres AP, Asano S, Ikeya T*, et al.* Identification of Phosphorus Sources in a Watershed Using a Phosphate Oxygen Isoscape Approach. *Environmental Science & Technology* 2019, **53**(9)**:** 4707-4716.

25. Yi R, Ishida T, Song PX, Ikeya T, Okuda N, Paytan A*, et al.* Using oxygen isotopes in phosphate to assess biological phosphorus cycling in a small and shallow freshwater lake system. *Limnology and Oceanography* 2024, **69**(5)**:** 1285-1298.

26. McLaughlin K, Silva S, Kendall C, Stuart-Williams H, Paytan A. A precise method for the analysis of δ18O of dissolved inorganic phosphate in seawater. *Limnology and Oceanography: Methods* 2004, **2**(7)**:** 202-212.

27. Li JY, Bai YG, Bear K, Joshi S, Jaisi D. Phosphorus availability and turnover in the Chesapeake Bay: Insights from nutrient stoichiometry and phosphate oxygen isotope ratios. *Journal of Geophysical Research-Biogeosciences* 2017, **122**(4)**:** 811-824.

28. Wang Z, Hattori S, Peng Y, Zhu L, Wei Z, Bao H. Oxygen Isotope Analysis of Nanomole Phosphate Using PO(3)(-) Fragment in ESI-Orbitrap-MS. *Anal Chem* 2024, **96**(11)**:** 4369-4376.

29. Wei Z, Wang B, Zhu L, Hong Y, Wang Z, Yan H*, et al.* A sub-liter pretreatment method for Orbitrap–based freshwater phosphate oxygen isotope measurement. *Applied Geochemistry* 2025, **194:** 106610.

30. Harke MJ, Gobler CJ. Global transcriptional responses of the toxic cyanobacterium, Microcystis aeruginosa, to nitrogen stress, phosphorus stress, and growth on organic matter. *PloS one* 2013, **8**(7)**:** e69834.

31. Billini M, Hoffmann T, Kuhn J, Bremer E, Thanbichler M. The cytoplasmic phosphate level has a central regulatory role in the phosphate starvation response of Caulobacter crescentus. *Commun Biol* 2024, **7**(1)**:** 772.

32. Zalatan JG, Catrina I, Mitchell R, Grzyska PK, O'Brien P J, Herschlag D*, et al.* Kinetic isotope effects for alkaline phosphatase reactions: implications for the role of active-site metal ions in catalysis. *J Am Chem Soc* 2007, **129**(31)**:** 9789-9798.

33. Stout LM, Joshi SR, Kana TM, Jaisi DP. Microbial activities and phosphorus cycling: An application of oxygen isotope ratios in phosphate. *Geochimica Et Cosmochimica Acta* 2014, **138:** 101-116.

34. Paytan A, Kolodny Y, Neori A, Luz B. Rapid biologically mediated oxygen isotope exchange between

water and phosphate. *Global Biogeochem Cy* 2002, **16**(1)**:** 13-11-13-18.

35. Gross A, Angert A. What processes control the oxygen isotopes of soil bio-available phosphate? *Geochimica et Cosmochimica Acta* 2015, **159:** 100-111.

36. Crombez H, Motte H, Beeckman T. Tackling Plant Phosphate Starvation by the Roots. *Developmental Cell* 2019, **48**(5)**:** 599-615.

37. Yang G, Deng M, Guo L, Du E, Zheng Z, Peng Y*, et al.* Characteristics of leaf nutrient resorption efficiency in Tibetan alpine permafrost ecosystems. *Nature Communications* 2025, **16**(1)**:** 4044.

38. Shinohara R, Hiroki M, Kohzu A, Imai A, Inoue T, Furusato E*, et al.* Role of organic phosphorus in sediment in a shallow eutrophic lake. 2017, **53**(8)**:** 7175-7189.

39. Zhang M, Xu D, Liu L, Wei Y, Gao B. Vertical Differentiation of Microplastics Influenced by Thermal Stratification in a Deep Reservoir. *Environmental Science & Technology* 2023, **57**(17)**:** 6999-7008.

40. Han X, Xun F, Zhu X, Zhao C, Luo W, Liu Y*, et al.* Mechanism of organic phosphorus transformation and its impact on the primary production in a deep oligotrophic plateau lake during stratification. *Water Research* 2024, **254:** 121420.

41. Davis CE, Mahaffey C. Elevated alkaline phosphatase activity in a phosphate-replete environment: Influence of sinking particles. *Limnology and Oceanography* 2017, **62**(6)**:** 2389-2403.

42. Colman AS, Blake RE, Karl DM, Fogel ML, Turekian KK. Marine phosphate oxygen isotopes and organic matter remineralization in the oceans. 2005, **102**(37)**:** 13023-13028.

43. Wasmund N. Probleme der spektrophotometrischen Chlorophyllbestimmung. *Acta hydrochimica et hydrobiologica* 2006, **12**(3)**:** 255-272.

44. Murphy J, Riley JP. A modified single solution method for the determination of phosphate in natural waters. *Analytica Chimica Acta* 1962, **27:** 31-36.

45. Liu Y, Wang J, Yang H, Jiang S, Jin Z, Chen J. Method for analyzing the oxygen isotope composition of HCl-extractable inorganic phosphate in sediments and soils. *Applied Geochemistry* 2021, **130:** 104978.

46. Chang SJ, Blake RE. Precise calibration of equilibrium oxygen isotope fractionations between dissolved phosphate and water from 3 to 37 °C. *Geochimica et Cosmochimica Acta* 2015, **150:** 314-329.

47. Zerkle AL, Kamyshny A, Kump LR, Farquhar J, Oduro H, Arthur MA. Sulfur cycling in a stratified euxinic lake with moderately high sulfate: Constraints from quadruple S isotopes. *Geochimica Et*

Cosmochimica Acta 2010, **74**(17)**:** 4953-4970.

48. Gao G, Zhu GW, Qin BQ, Chen J, Wang K. Alkaline phosphatase activity and the phosphorus mineralization rate of Lake Taihu. *Science in China Series D-Earth Sciences* 2006, **49**(S1)**:** 176-185.

49. Doig LE, North RL, Hudson JJ, Hewlett C, Lindenschmidt KE, Liber K. Phosphorus release from sediments in a river-valley reservoir in the northern Great Plains of North America. *Hydrobiologia* 2017, **787**(1)**:** 323-339.

50. Chen Q, Chen J, Wang J, Guo J, Jin Z, Yu P*, et al.* In situ, high-resolution evidence of phosphorus release from sediments controlled by the reductive dissolution of iron-bound phosphorus in a deep reservoir, southwestern China. *Sci Total Environ* 2019, **666:** 39-45.

Table 1. Used parameters and fitted results in a one-dimensional transport-reaction model

Parameters	Definition	Unit	Lake Hongfeng	Lake Aha	reference
D	Diffusion coefficient	m^2/h	0.0036	0.0036	Zerkle et al., 2010
$K_{PO_4^{3-}}$	Half-saturation constant for PO_4^{3-}	-	0.10	0.10	Gao et al., 2006
K_{Chla}	Half-saturation constant for Chla	-	0.05	0.05	Gao et al., 2006
k_s	Sediment PO_4^{3-} release rate constant	1/h	0.016	0.10	Doig et al., 2017; Chen et al., 2019
μ_{max}	Maximum specific growth rate of algae	1/h	0.18	0.44	Fitted result
k_{org}	Organic P mineralization rate constant	1/h	0.11	0.16	Fitted result
$AKIE_{uptake}$	*AKIE* during PO_4^{3-} uptake	-	0.9932	0.9929	Fitted result
$AKIE_{org}$	*AKIE* for organic P mineralization	-	0.9906	0.9900	Fitted result
$\delta^{18}O_P$ (sediment)	$\delta^{18}O_P$ value from sediment	‰	17.1	15.7	This study

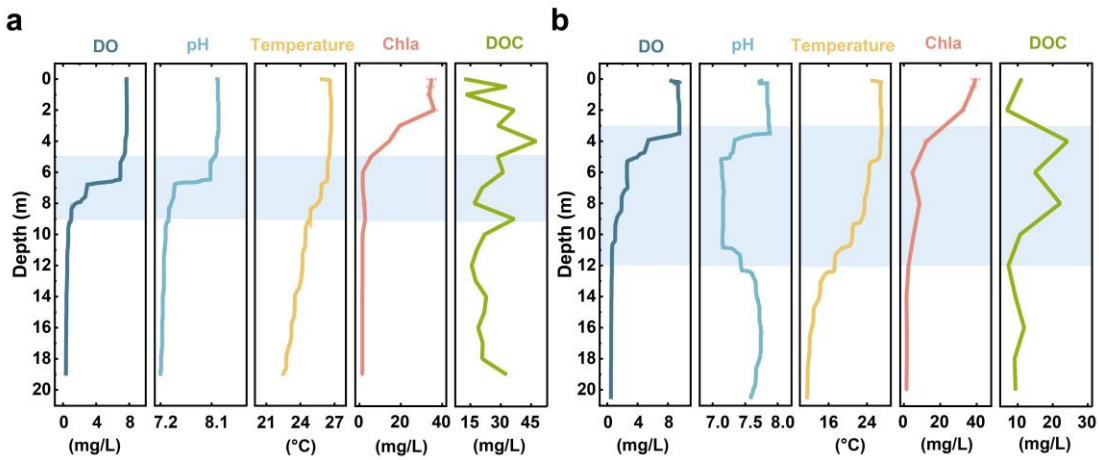

Fig. 1 Profiles of DO, pH, T, Chla, and DOC. The blue shaded area represents the thermoclines in the lakes. **a,** Lake Hongfeng, **b,** Lake Aha.

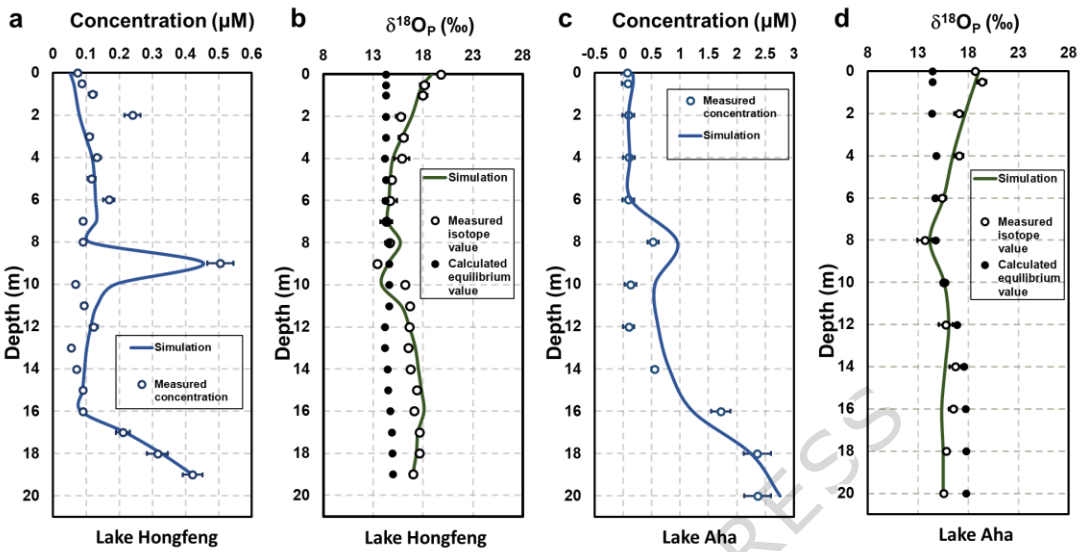

Fig. 2 The fitting results of a one-dimensional vertical diffusion model for PO_4^{3-} concentration and the $\delta^{18}O_P$. Open dots represent the measured $\delta^{18}O_P$ values, filled dots represent the calculated equilibrium $\delta^{18}O_P$ values according to equation (2), and the lines represent the fitted values. **a,** PO_4^{3-} concentration in Lake Hongfeng; **b,** $\delta^{18}O_P$ in Lake Hongfeng; **c,** PO_4^{3-} concentration in Lake Aha; **d,** $\delta^{18}O_P$ in Lake Aha.

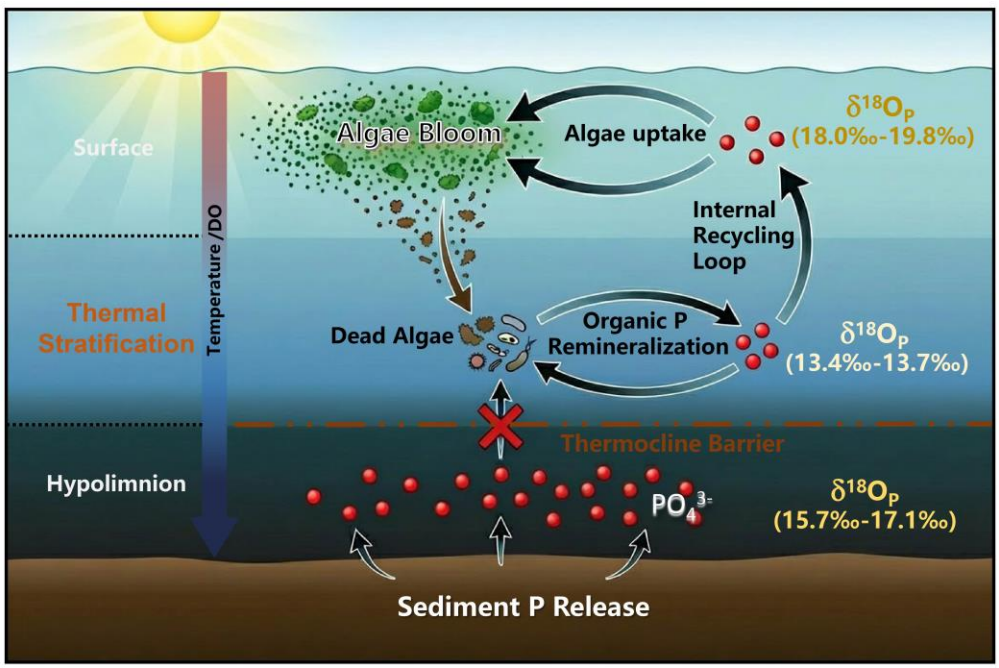

Fig. 3 A schematic diagram of the P cycle dynamics in thermally stratified lakes during eutrophication

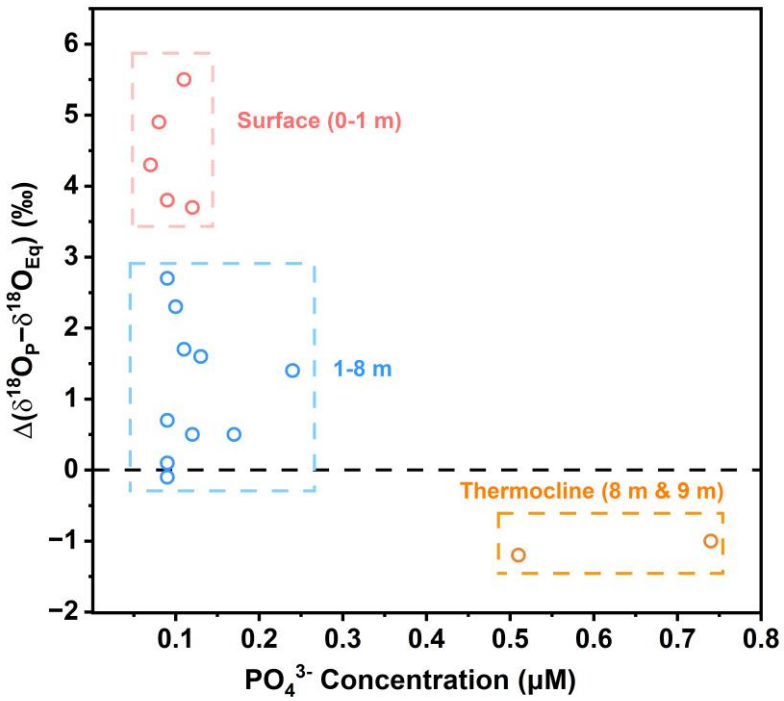

Fig. 4 The relationship between the deviation of measured $\delta^{18}O_P$ from the equilibrium value ($\Delta(\delta^{18}O_P$-$\delta^{18}O_{Eq}=\delta^{18}O_P - \delta^{18}O_{Eq}$) and the PO_4^{3-} concentration from the surface to the thermocline (0-9 m).

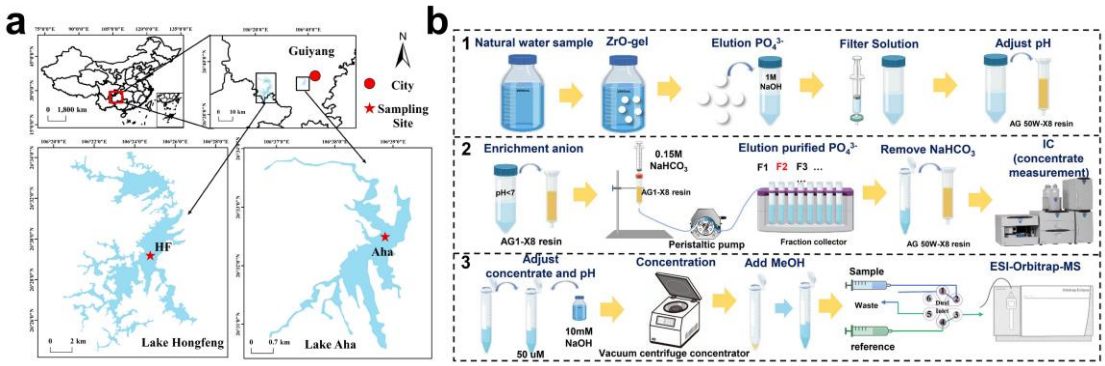

Fig. 5 Map of sampling locations and the sample preparation protocol for $\delta^{18}O_P$ analysis. a, Map of sampling sites in Lake Hongfeng and Lake Aha. **b,** the pretreatment protocol for purifying PO_4^{3-} from lake water for ESI-Orbitrap-MS $\delta^{18}O_P$ measurement.

Editorial summary:
Rapid remineralization of organic phosphorus near the thermocline supplies phosphate to upper layers, promoting rapid algal growth during summer stratification, according to high-resolution vertical phosphate oxygen-isotope analyses in two low-phosphorous lakes in China.

Peer review information:
Communications Earth and Environment thanks Andrew C. Smith, Daniel Graeber and the other, anonymous, reviewer(s) for their contribution to the peer review of this work. Primary Handling Editors: Mengru Wang and Nicola Colombo. A peer review file is available